Low-temperature specific heat and thermal conductivity of a glassy polymer under applied pressure

J. M. Grace* and A. C. Anderson
Department of Physics, University of Illinois at Urbana-Champaign, 1110 West Green Street, Urbana, Illinois 61801
(Received 26 January 1989)

The low-temperature thermal properties of an amorphous polymer were used to probe glassy behavior as a function of pressure. Specifically, the thermal diffusivity a and thermal conductivity κ of an epoxy were measured over the range 0.3–10 K at pressures up to roughly 4 kbar. The specific heat determined from κ/a was observed to decrease with pressure; the relative changes were rather uniform over the entire temperature range. The thermal-conductivity measurements revealed an increased conductivity with pressure for temperatures above 1 K. The magnitude of this pressure-induced increase in κ was smaller at lower temperatures; near 0.3 K, the measurements indicated decreased κ as pressure was applied. Analysis of these measurements using the tunneling model suggests that the energy density of two-level excitations decreases with pressure, while the coupling of these excitations to phonons increases. The measured changes in the 0.3–1-K regime indicate that the density of two-level systems depends on the phonon velocity v as v^{-3}. The magnitude of the pressure-induced changes in the range 1–10 K suggests that the strong phonon scattering and excess excitations in this regime are most likely not related to structural length scales in the glass. Finally, the similar changes with pressure over the entire temperature range suggest that all the excitations, namely phonons, two-level systems, and the additional modes above 1 K, are related. These results are discussed with regard to the tunneling model, microscopic models, and the fracton theory.

I. INTRODUCTION

The low-temperature thermal properties of glasses reveal interesting behavior that has become recognized as a signature of disorder in solids. We have investigated the effects of pressure (0–4 kbar) on the low-temperature (0.3–10 K) thermal conductivity and specific heat of an epoxy-resin, a representative amorphous (glassy) polymer. The goal of this work was to examine the strain dependence of low-energy excitations and, in addition, to test some current models relevant to glassy phenomena in the temperature region of 1–10 K.

At temperatures below ≈ 1 K the specific heat C of a dielectric amorphous solid can be 2 orders of magnitude greater than the corresponding crystalline specific heat, while the thermal conductivity κ can be 3 or 4 orders of magnitude smaller for the glass than for the crystal. The specific heat, which is quasilinear in temperature T, is indicative of localized excitations which are present in addition to phonons. These excitations scatter phonons, giving rise to a reduced, $\sim T^2$ thermal conductivity. A universal feature of glasses appears to be that the phonon mean free path is of the order of 150 phonon wavelengths in this T^2 regime.[1–3]

In addition to low-temperature specific-heat and thermal-conductivity measurements, many other experimental investigations of glasses have been performed.[3] From this body of information, some important characteristics of the low-energy excitations have been determined. Saturable acoustic attenuation[4] of amorphous solids indicates that a two-level description of these excitations suffices to explain phenomena observed below 1 K and, thus, permits a mapping onto the problem of a spin-$\frac{1}{2}$ particle in a magnetic field.[3]

A phenomenological model, in which it is assumed that some entity of atomic dimensions tunnels between two potential wells,[5,6] can account for two-level systems (TLS's) and the phenomena below 1 K. As will be discussed, thermal measurements probe the density of TLS's and their coupling to phonons. Information about the pressure dependence of the TLS's—their density and phonon coupling—may increase our understanding of these ubiquitous excitations.

In the temperature range $1 \lesssim T \lesssim 10$ K, amorphous solids exhibit a nearly temperature-independent "plateau" in thermal conductivity and also a broad maximum (or "bump") in C/T^3. The plateau in κ is indicative of strongly-frequency-dependent phonon scattering; the broad maximum in C/T^3 is the result of a large increase in the density of states $N(\omega)$ at high frequencies. An empirical correlation is that glasses having the plateau at higher temperatures have the bump in C/T^3 also at higher temperatures.[7] It therefore has been speculated that these two "high-temperature" features are related to each other[7,8] and, perhaps, also to the lower-temperature, TLS behavior.[9,10]

The bump and plateau phenomena have been the focus of recent theoretical work. An elegant but controversial theory of fractons relates the two features to a critical length scale below which the amorphous solid is assumed to exhibit self-similar geometry.[11] There are also microscopic models that relate the bump and plateau to vibrational modes of molecular structures.[12,13] Pressure measurements of the bump and plateau should provide a test

for the self-similarity idea; compressing a sample would correspond to decreasing the supposed critical length scale. In addition, the pressure measurements should be useful in assessing the microscopic models.

A brief discussion of the various models is given below. More detailed explanations can be found in the references cited.

A. $T \lesssim 1$ K: The tunneling model

To account for glassy behavior below ≈ 1 K, the tunneling model[5,6] was introduced. This model postulates that the interatomic potential in structurally disordered solids contains regions having two nearly identical wells separated by barriers of height V_0 and having asymmetries Δ. An atomic- or molecular-size object is assumed to reside at a given double-well site. Tunneling of this object through the barrier gives rise to an energy splitting Δ_0 of the ground state if the potential wells are symmetric. For asymmetric wells the TLS energy splitting is $E=(\Delta^2+\Delta_0^2)^{1/2}$.

A consequence of the expected distributions in Δ and V_0 is a broad distribution of the TLS energies E and a broad distribution in the TLS relaxation rate τ^{-1}. Therefore, the measured specific heat will depend on an experimental time scale t, and the TLS distribution $P(E,\tau^{-1})$ must be considered in computing the TLS contribution to the specific heat. The TLS contribution to the specific heat is[14]

$$C_{\rm TLS}=k_B\int dE\int_{t^{-1}}^{\tau_{\rm min}^{-1}}P(E,\tau^{-1})\left[\frac{E}{2k_BT}\right]^2 \times\operatorname{sech}^2\left[\frac{E}{2k_BT}\right]d\tau^{-1}\ , \tag{1}$$

with

$$P(E,\tau^{-1})=\frac{\bar{P}/2\tau^{-1}}{[1-(\tau^{-1}/\tau_{\rm min}^{-1})]^{1/2}}\ , \tag{2}$$

where $\bar{P}$ is a constant and where $\tau_{\rm min}$ is given by

$$\tau_{\rm min}^{-1}=\sum_i\frac{\gamma_i^2E^3}{2\pi\hbar^4\rho v_i^5}\coth\left[\frac{E}{2k_BT}\right]\ . \tag{3}$$

Here, i labels the phonon mode, v is a phonon velocity, $\gamma=\frac{1}{2}(\partial\Delta/\partial e)$ is the TLS-phonon coupling constant (i.e., $2\gamma e$ is the change in Δ induced by strain e), ρ is the mass density of the glass, and k_B is the Boltzmann constant.

Equation (1) gives

$$C_{\rm TLS}=\frac{\pi^2}{6}k_B^2nT\ , \tag{4}$$

where $n=n(E)$ is the roughly constant energy density of TLS's and represents the integral of $P(E,\tau^{-1})$ over τ^{-1}:

$$n=\frac{\bar{P}}{2}\ln\left[\frac{4t}{\tau_{\rm min}}\right]\ . \tag{5}$$

The time $\tau_{\rm min}$ is evaluated at $E\approx 2k_BT$. If t is longer than $\tau_{\rm max}$, the equilibration time of the slowest relaxing TLS, the integrated density n becomes

$$n=\frac{\bar{P}}{2}\ln\left[\frac{4\tau_{\rm max}}{\tau_{\rm min}}\right]\ . \tag{6}$$

Typically, $n/\bar{P}\approx 10$.

The phonon lifetimes (and, therefore, the thermal conductivity) below 1 K can be calculated by considering the resonant interaction of phonons with the localized TLS's. The TLS and phonon relaxation rates are

$$\tau_{\rm TLS}^{-1}\sum_i\frac{\gamma_i^2\Delta_0^2E}{2\pi\hbar^4\rho v_i^5}\coth\left[\frac{E}{2k_BT}\right] \tag{7}$$

and

$$\tau_i^{-1}({\rm phonon})=\frac{\pi\gamma_i^2}{\hbar\rho v_i^2}\left[\frac{\Delta_0}{E}\right]^2n(E)\hbar\omega\tanh\left[\frac{E}{2k_BT}\right]\ . \tag{8}$$

The quantity Δ_0/E is a measure of the symmetry of a double-well site. For maximum symmetry $\Delta=0$; hence, $\Delta_0/E=1$. TLS's arising from these symmetric double wells couple most strongly to phonons and have the dominant effect on κ. The phonon mean free path due to this resonant scattering is given by

$$l_i^{-1}(\omega)=\frac{\pi\gamma_i^2}{\hbar\rho v_i^3}\bar{P}\hbar\omega\tanh\left[\frac{\hbar\omega}{2k_BT}\right]\ . \tag{9}$$

From $l_i^{-1}(\omega)$ the thermal conductivity can be calculated:

$$\kappa(T)=\tfrac{1}{3}\sum_i\int C_i(\omega)v_i(\omega)l_i(\omega)d\omega\ , \tag{10}$$

where $C(\omega)$ is the phonon contribution to the specific heat at frequency ω. For constant v, with $l_i^{-1}(\omega)$ as given in Eq. (9), the integral gives

$$\kappa(T)\propto\left[\frac{\rho v}{\bar{P}\gamma^2}\right]T^2\ . \tag{11}$$

Here, v and γ represent appropriate averages over the acoustic-phonon modes.

It has been shown above that the linear temperature dependence of C and the quadratic temperature dependence of κ can arise from the TLS's and their resonant scattering of phonons, respectively. It should be mentioned that experiments below 1 K reveal[15] $C\propto T^{1+\alpha}$ and $\kappa\propto T^{2-q}$, where $0.1<\alpha<0.5$ and $q\approx 0.2$. The superlinear dependence of C on T is readily understood from the time dependence expressed in Eq. (5). The distribution responsible for this time dependence, $P(E,\tau^{-1})$, can also give rise to the subquadratic dependence of κ on T. It is also possible that variations from the assumed distribution of Δ and V_0 among the TLS's contribute to this behavior.

The broad range of $\tau_{\rm TLS}$ has consequences for specific-heat measurements performed at angular frequency Ω. To understand the frequency dependence it is helpful to consider first a single TLS characterized by single values of E and τ. If a TLS is coupled to a heat bath having a sinusoidally time-varying temperature, the effective

specific heat is a complex number,

$$C^*=C^*(E,\tau^{-1})=\frac{C_{\rm TLS}(E)}{1+i\Omega\tau}\ , \tag{12}$$

where $C_{\rm TLS}(E)$ is the total (long-time) specific heat of the TLS. Now the effects of a distribution $P(E,\tau^{-1})$ can be calculated by integrating $C^*(E,\tau^{-1})$ over the distribution:

$$C^*(T,\Omega)=\int\frac{C_{\rm TLS}(E)}{1+i\Omega\tau}P(E,\tau^{-1})d\tau^{-1}\,dE=2k_B^2T\int_0^{X_{\max}}dX\,X^2{\rm sech}^2(X)\int_{\tau_{\max}^{-1}}^{\tau_{\min}^{-1}}d\tau^{-1}\frac{P(E,\tau^{-1})}{1+i\Omega\tau}\ , \tag{13}$$

where $X=E/2k_BT$.

It should be noted that the tunneling model is phenomenological, having adjustable parameters $\bar{P}$ and γ. No indication as to the microscopic origin of the TLS's is provided nor does the model explain the universal character of glassy behavior. Nonetheless, it can be helpful to investigate how $\bar{P}$ and γ are influenced in a controlled experiment.

If the coupling parameter γ is known, a simple estimate of the effect of pressure can be made. A typical value for γ is ≈ 1 eV (e.g., vitreous silica[6]). If the modulus of compression of the glass is ~ 670 kbar (1 kbar $\approx 10^8$ Pa), then a pressure of 1 kbar would induce a strain $\mathbf{e}\sim 0.0015$ and the product $\gamma\mathbf{e}$ then would be ~ 0.0015 eV or 18 K. Hence, a change in Δ of roughly 40 K would be induced if γ remained constant. Such a change in Δ would result in a large change in a TLS energy E that was formerly of order 1 K. Considering that thermal measurements below 1 K probe TLS's having energies of order 1 K or less, one might conclude that most of the TLS's in the experimental window of observation are moved out to ~ 40 K by the applied pressure. A gap in $n(E)$ below 1 K would result if all energies E were increased by pressure. There is, of course, the possibility that some TLS's have negative values of γ so that TLS's at higher energies would be moved into the 1-K range, thereby filling in the gap. It is also possible that, for strains so many times larger than those associated with phonons, the linear relation between Δ and $\mathbf{e}$ may not hold.

Independent of the tunneling model or other theoretical models, one can make the following observation, provided the sample remains amorphous upon application of pressure. Since all amorphous solids have roughly the same thermal conductivity (and, more loosely, the same specific heat), the application of pressure is not expected to cause a large change in either κ or C at temperatures below 1 K.

B. $1 \lesssim T \lesssim 10$ K: Librations, rotations, and fractons

The "bump" in C/T^3 is indicative of a rise in the density $N(\omega)$ of vibrational excitations. The "plateau" in thermal conductivity is a consequence of strong phonon scattering[2] at high frequencies or short wavelength λ; that is, $l\propto\omega^{-4}\propto\lambda^4$. (Essentially, amorphous solids are low-pass phonon filters.)

Among the first observations about the bump and plateau phenomena is that these two features have similar onset temperatures for a given amorphous solid.[7,16] In other words, the energy scales for the bump and for the plateau appear to be correlated. Two ideas proposed for a common origin of these features are (i) a TLS density $n(E)$ having a term quadratic[8,10] in E, and (ii) phonon dispersion.[7,8] The quadratic term in $n(E)$ has no obvious justification, and there is no direct evidence for such behavior. As for phonon dispersion, measurements on vitreous silica[16,17] reveal no dispersion at frequencies corresponding to the plateau in κ.

There also have been some ideas put forth that attempt to explain the plateau but do not address the bump in C/T^3. The essential ingredient for a theory of the plateau is a mechanism for strongly-wavelength-dependent phonon scattering.[18] Various forms of structure scattering have been proposed (e.g., density, velocity, and force-constant fluctuations), but none can account for the magnitude of scattering required[7] to produce a plateau in κ.

More recent work has produced microscopic models[12,13] for the well-characterized systems vitreous SiO_2 and crystalline $KBr_{1-x}(CN)_x$. $KBr_{1-x}(CN)_x$ is an orientational glass over a range of x. The orientational disorder arises because the CN impurities doped into a KBr crystal can have random orientations at their sites.[19,20] In contrast, vitreous silica is a typical structurally disordered solid; the SiO_2 molecules have an arrangement characterized by short-range order and the absence of long-range order. Both substances have a relatively simple molecular structure, so that microscopic modeling can be attempted.

The CN concentration x in $KBr_{1-x}(CN)_x$ can be varied over a broad range.[19] For low concentrations the CN molecules behave as isolated impurities within an ordered crystalline lattice. At higher CN concentrations ($x\approx 0.5$) the substance exhibits glassy low-temperature behavior. Such a material creates the possibility of observing behavior through a transition from a system of isolated impurities to an orientational glass. The glassy samples exhibit the characteristic bump and plateau features, as well as the TLS-related phenomena.[20]

A recently proposed model[12] considers the TLS in $KBr_{1-x}(CN)_x$ as understood and focuses on explaining the bump and plateau. (The TLS can be interpreted as arising from the tunneling motion of interacting CN; hence, a microscopic model relating the bump and plateau to CN motion also links these features to the lower-temperature TLS behavior.) The authors of the model consider small-angle oscillations, or "librations," of interacting CN. To carry out calculations on the KBr-KCN system, the CN are modeled as interacting elastic dipole defects placed randomly in an elastic continuum.

From this model the calculated specific heat is in fair agreement with available data (the calculation and experiments differ by $\sim 25\%$), but the plateau thermal conductivity, as calculated, is a factor of 2 or 3 larger than the measurements. Although the agreement is only qualitative this microscopic theory of librational modes of CN does provide a way to link the bump and plateau. Furthermore, there would be some hope for relating the bump and plateau to the TLS behavior.

With the simple picture of elastic dipole defects, one can make qualitative predictions about the effects of pressure on the bump and plateau. As applied pressure tends to stiffen a material,[21] the normal modes of the elastic dipole defects might also be stiffened [i.e., the onset of the rise in $N(\omega)$ would be shifted to higher ω]. The bump in C/T^3 would then be reduced in magnitude as the associated excitations moved to higher energies. Furthermore, as these librational modes were shifted to higher ω, the phonon scattering in the plateau would be reduced, thereby increasing the conductivity in the plateau. Thus, the microscopic model of $KBr_{1-x}(CN)_x$ suggests that applied pressure will reduce the bump while increasing the plateau conductivity.[22]

A detailed microscopic model relevant to vitreous silica has evolved from neutron-scattering measurements of the excitations responsible for the bump in C/T^3. These measurements[9,13] indicate a large density of harmonic excitations in the range 0.3–4 THz. The model assumes that these excitations correspond to relative rotation of SiO_4 tetrahedra. The calculated form of scattered intensity as a function of wave vector is quite similar to the experimental results. Also, the temperature dependence of the specific heat from 5 to 20 K, as calculated from the neutron-scattering data, agrees with that directly measured in the same temperature range.

The model of rotating tetrahedra has not been used to calculate thermal transport in the plateau; hence, no information is available on the potential for this structural model to link the bump and plateau phenomena. However, speculations as to the relevance of the model to TLS's have been made.[9,13] Computations suggest that a structure based on linked tetrahedra can have an excitation spectrum with a low-frequency range characterized by double-well potentials.[23,24] The implication is that the TLS and the bump may arise from the respective low- and high-frequency vibrational modes of the same structure.

From the above ideas regarding vitreous silica, one can make qualitative predictions as to the effect of pressure on the low-temperature specific heat of glass. If the TLS and bump are linked as described above, one would expect that a stiffening of the molecular structure would shift the bump excitations to higher frequencies and broaden the TLS distribution. The shift of the bump excitations is easily understood as an increase in the frequencies associated with the normal modes of the vibrating structure (i.e., the linked, rotating tetrahedra). The broadened TLS distribution perhaps requires some explanation. In the discussion of TLS's, a broad distribution $n(E)$ was used to derive $C \propto T$. In principle, this broad distribution should have some high-energy limit, $E_{\max}$, corresponding to where the nature of the vibrational excitations changes from highly anharmonic to harmonic. In other words, this limit should be in the bump regime. If the total number of excitations ($\approx nE_{\max}$) remains constant, but $E_{\max}$ increases as the material stiffens, one would expect n to decrease. In short, considering the structural model proposed for vitreous silica, one might expect that applied pressure would cause a reduction of the bump in C/T^3 and a drop in the TLS contribution to the specific heat.

Whereas the above-mentioned microscopic models use an analysis of molecular structure to predict the low-temperature behavior of specific disordered solids, the fracton theory makes a general statement that all amorphous material should exhibit a crossover from phonon behavior to fracton behavior.[11] The universal glassy behavior at $T \approx 1-10$ K is then attributed to the crossover. This thinking was inspired to a large extent by the known frequency dependence of phonon scattering in glasses. The strong phonon scattering, corresponding to the plateau in thermal conductivity, and the subsequent short mean free paths at high frequencies, are indicative of phonon localization. Because of its use of geometrical arguments to explain this universal localization, the phonon-fracton crossover idea is quite attractive.

Some basic consequences of the phonon-fracton crossover have been presented[25] as scaling relations, involving a crossover frequency ω_{co}, a crossover length scale ξ, and sound velocity v. These relations are

$$\omega_{co} \propto \xi^{-(1+\theta/2)} , \tag{14}$$

$$v \propto \xi^{-\theta/2} . \tag{15}$$

The parameter θ is an exponent used to describe the range dependence of the diffusion constant on a fractal network.[26] The crossover frequency is the frequency at which the density of states changes from phonon ($\propto \omega^2$) to fracton ($\propto \omega^{\bar{\bar{d}}-1}$) behavior. The spectral (fracton) dimension $\bar{\bar{d}}$ is analogous to the Euclidean dimension in that the vibrational density of states in Euclidean dimension n is proportional to ω^{n-1}. This spectral dimension is given by

$$\bar{\bar{d}} = 2D/(2+\theta) , \tag{16}$$

where D is the Hausdorff (fractal) dimension, which has a value between the topological dimension and the Euclidean dimension. (For example, a random walk in a plane fills a Euclidean dimension of $n=2$, but the curve indicating the motion of the random walk is a one-dimensional object embedded in the Euclidean space; the dimension D of such a random walk lies between 1 and 2.)

There is strong evidence that fractons have been observed in silica aerogels;[27,28] however, these low-density materials are not representative glasses. The aerogels have a rarefied structure with a broad range of pore sizes. Even for such low-density (~ 100 kg/m^3) materials, the range of fractal behavior is limited to only 1 order of magnitude in length scale.[29] This range in length scales is determined by the relative sizes of the pores in the material and the clusters from which the material is formed.

For the bulk glasses (having typical densities of 2000 kg/m^3), one would expect a rather limited range in length scales over which fractal geometry exists (for example, expected "pore" diameters in vitreous silica[30] are roughly 2–4 Å; the SiO_4 tetrahedra are not considerably smaller than these "pores"). Although the phonon-fracton crossover explanation of glassy behavior is elegant, the use of a theory of fractons for materials that most likely have no appreciable fractal structure is questionable.

One could argue that the relevant length scales are dynamical and not structural; the above-mentioned small range of structural length scales over which a glass could be fractal might then be irrelevant. In addition, one might argue that amorphous polymers (which behave as typical glasses) have a fractal character arising from the random configuration of long molecular chains. Indeed, there have been claims[31] by some that thermal measurements on epoxies[32] support the fracton theory of glasses. Others, however, have suggested nonfractal explanations for the same data.[32,33] In short, there has been no conclusive proof or refutation of the relevance of the phonon-fracton crossover to glasses.

For the purposes of this study, the fracton theory will be treated in a general context as a theory of localization. The qualitative effects of pressure can be estimated as follows. By reducing the sample volume, the critical length scale ξ should decrease. This decrease in ξ would correspond to an increase in the crossover frequency ω_{co}. If the "bump" in C/T^3 arises from this crossover, then its magnitude should decrease as the crossover shifts to higher energies. In addition, if the plateau is related to phonon localization at the phonon-fracton crossover, then the plateau conductivity should rise as the fractons move to higher energies. The degree of change in the specific heat and the thermal conductivity depend on the magnitudes of the various dimensions and parameters mentioned above. Estimates of these parameters indicate[34] that the scaling exponents should be of order unity; therefore the changes in plateau and bump for small length changes are expected to be small.

C. Previous measurements

Experiments at low temperatures and high pressures are rather difficult to perform. It is therefore not surprising that only a limited amount of such data are available for amorphous solids. Attempts have been made to observe changes in the low-temperature properties of glass samples strained permanently by, for example, ion exchange at the surfaces.[35] The low-temperature properties of such samples were identical to those of unstrained samples, perhaps because the "average" deformation in these strained samples was close to zero.

Two materials that have been studied under homogeneous pressures of a few kbar at low temperatures are Teflon[36] and vitreous silica.[37] Teflon has been employed as a pressure-transmitting medium[38] for low-temperature, high-pressure calorimetry. A knowledge of the pressure dependence of the specific heat of Teflon is therefore essential to obtaining reliable specific-heat data for other samples. Boyer *et al.*[36] have measured the low-temperature ($\sim$1–20 K) specific heat of Teflon at pressures to $\sim$5 kbar, corresponding to a decrease of roughly 8% in volume. The most notable pressure effect on the Teflon specific heat is the dramatic reduction of the bump in C/T^3; near the maximum in C/T^3 the total specific heat is reduced by more than a factor of 2 at a pressure of 5.2 kbar. The measurements do not extend below 1 K where the TLS dominate the specific heat.

Interpretation of the experimental results is complicated because of questions as to the importance of the partial crystallinity of the Teflon sample. In the measurements, pressure is applied at room temperature and could affect the degree of partial crystallinity in the Teflon. Thus, the experiment may not be measuring intrinsic glassy behavior as a function of pressure. Dobbs and Anderson[39] make a comparison with their low-temperature measurements of thermal expansion α and find a discrepancy in the thermodynamic quantity $[\partial(C/T^3)/\partial P]_T$. This derivative, when evaluated near 2 K, is a factor of $\sim$3 greater for the specific-heat measurements than for the thermal-expansion measurements. The partial crystallinity of Teflon, and the fact that a phase transition occurs in Teflon at low pressures[39] near 300 K, may account for the discrepancy between the two sets of measurements.

Boyer *et al.* analyze the specific-heat data in terms of a T^3 (predominantly phonon) contribution, and contributions from two Einstein terms. In this context, both the phonon contribution and the Einstein contribution decrease as pressure increases. These two phenomena are interpreted as a stiffening of the sample and an upward shift of the Einstein temperatures, respectively.

Vitreous silica has also been studied under pressure at low temperature. Bartell and Hunklinger[37] have measured the acoustic absorption of Suprasil W1 (a quartz glass) at a pressure of 1.2 kbar in the temperature range 0.4–4 K at a frequency of 200 MHz. They report a $\sim$25% increase in acoustic absorption. According to the tunneling model,[40] the acoustic absorption is proportional to the term $\bar{P}\gamma^2$. Hence, the increase in acoustic absorption for vitreous silica can be interpreted as an increase in the TLS-phonon coupling as pressure increases. Furthermore, if γ is roughly constant, a pressure of 4 kbar in vitreous silica should induce a change $\sim$150 K in a given double-well asymmetry Δ. However, the TLS energies probed in the ultrasonic experiments are less than 1 K. Therefore, the large changes in TLS asymmetries that should be induced by the applied pressure appear to leave a TLS distribution that has roughly the same density near the low-energy (<1 K) window of observation. Thus, the relatively small change (25%) in acoustic absorption might indicate[37,41] that there are nearly as many double wells with a positive γ as with a negative γ.

II. EXPERIMENTAL CONSIDERATIONS

As can be inferred from the preceding section, a reasonable choice of sample would be an entirely amorphous polymer that does not crystallize upon cooling or upon application of pressure. Such crystallization is inhibited by high crosslink densities in amorphous polymers.[42] Some common highly crosslinked amorphous po-

lymers are the epoxy resins.[43]

There are a variety of epoxy resins that have been studied as representative glasses.[44,45] In particular, some Scotchcast resins have been studied at the University of Illinois, and a body of zero-pressure, low-temperature data for thermal conductivity, specific heat, and phonon velocity exists.[44] The number-8 Scotchcast resin (SC-8) has a high compressibility ($\sim 1-2\%$ per kbar at room temperature) and is easy to cast and machine. High compressibility is desirable for creating appreciable strain $\mathbf{e}$ at lower pressures and thus facilitates making a large deformation term $2\gamma\mathbf{e}$. The additional advantages of using a "glue" for a sample will become apparent in the discussion of sample preparation. Although details of the molecular structure of SC-8 are not available, the fact that the material has been well characterized as glassy[46] and the fact that glassy properties depend only weakly on chemical composition justifies the use of SC-8 in this experimental investigation.

Experimental work that combines high pressures and low temperatures presents a number of technical challenges, and the choice of measurement technique becomes quite limited. In addition, the applied pressure may vary with temperature and must be determined for the low temperatures at which measurements are made. A third consideration is that the electrical components and leads needed for the measurement must withstand high pressures and thermal cycling, as must their feedthroughs out of the pressure cell.

For high pressures a cylindrical geometry is most convenient, as a simple piston arrangement can be used to apply pressure. For construction of the pressure cell, a high-strength, high-thermal-conductivity material such as a beryllium-copper alloy must be employed. However, below 1 K the metallic pressure cell can have a heat capacity more than 100 times greater than the glassy sample to be studied.[36] Hence, a cell-independent determination of sample specific heat is necessary. Such cell-independent techniques probe the flow of heat into or out of the sample. Some examples are hot-wire techniques,[47–49] transient-diffusivity measurements,[50] and ac steady-state measurements of thermal diffusivity.[51]

An analysis of the above techniques, with consideration of the thermal-boundary impedance[52] arising between different materials at low temperatures, led to the choice of the ac steady-state diffusivity technique. An added benefit of this choice is that the requisite two thermometers and heater can also be used for dc radial heat-flow measurements of the thermal conductivity.[51,53]

A. Radial heat-flow measurement of conductivity

A standard technique for measuring thermal conductivity is to apply a known heat current to a thermally anchored sample and measure the resulting temperature gradient between two points in the sample.[54] For a cylindrical geometry as shown in Fig. 1, the sample is thermally grounded at its outer radius R and power $\dot{Q}$ is supplied by an axial heater. The resulting temperature distribution is probed at radii r_1 and r_2. The ratio $\Delta T_{1,2}/\dot{Q} \equiv [T(r_1)-T(r_2)]/\dot{Q}$ is Z_{r_1,r_2}, the thermal impedance of a shell of sample of inner radius r_1 and outer radius r_2. From this quantity, κ is determined from

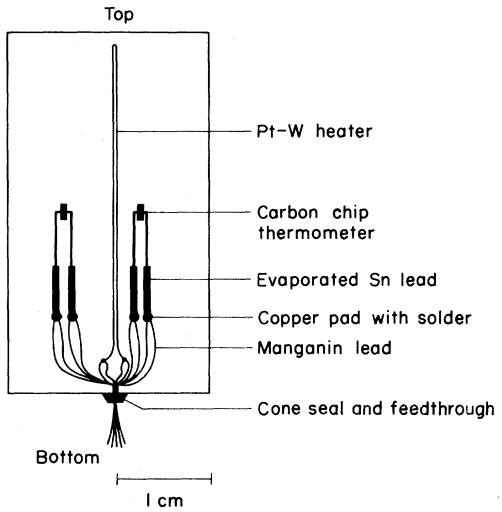

FIG. 1. Cylindrical sample—view of semicylinder before reassembly.

$$\kappa = -\frac{\dot{Q}\ln(r_1/r_2)}{2\pi l \Delta T_{1,2}} = \frac{\ln(r_2/r_1)}{2\pi l Z_{r_1,r_2}}\ , \tag{17}$$

provided the length l is much larger than r.

The effect of finite sample and heater lengths is to change the relation between the apparent thermal impedance and the thermal conductivity, i.e., Eq. (17) is no longer correct. Calculations of this effect are described in Ref. 55. If thermal contact is made to the end faces of the cylinder, the boundary conditions at these faces must be considered. As a worst case one can consider the entire surface of the cylinder to be at temperature T_0. When this boundary-value problem is solved for the sample dimensions and positions of heater and thermometer chosen for the measurements on SC-8, the effect of making thermal contact to the ends (as in the actual experiment) is found to be small. Use of Eq. (17) instead of the solution for the finite sample would result in an error in κ of roughly $+3\%$. This result is for zero pressure (an uncompressed sample). In addition to this finite-size effect at zero pressure, there is a further effect if the sample is compressed. The heater length l will contract by the same fraction as the sample length L. If the value of l is properly corrected for compression, it is found that there is an additional error of roughly $+0.1\%$ for each percent compression of sample length (for compression $\lesssim 10\%$). In brief, the thermal conductivity is well approximated by Eq. (17).

B. Thermal-diffusivity measurements

The sample arrangement used for thermal conductivity measurements can also be used for ac, steady-state thermal-diffusivity measurements. An oscillating power of the form $P_0(1-e^{i\Omega t})$ is applied to the heater. Thermometers T_1 and T_2 register the ac temperature disturbances at r_1 and r_2, respectively. From the relative am-

plitudes and phases of the signals at r_1 and r_2 the thermal diffusivity can be calculated. A brief description of this technique is given below; a more detailed discussion can be found in Refs. 51 and 55.

A calculation of the effects of the ac heater power at a given radius r requires the solution of Poisson's equation: $\nabla^2 T = \alpha^{-1} \partial T/\partial t$, where α $(=\kappa/C)$ is the thermal diffusivity. This solution has both dc and ac terms:

$$T(r,t) = T_{\rm dc}(r) + T_{\rm ac}(r,t) , \tag{18}$$

$$T_{\rm dc}(r) = T_0 - \frac{P_0}{2\pi l \kappa} \ln(r/R) ,$$

$$T_{\rm ac}(r,t) = \{F[K_0(\eta_r \sqrt{i}) - D I_0(\eta_r \sqrt{i})] e^{i\Omega t}\} ,$$

where $\eta_r \equiv r\sqrt{\Omega/\alpha}$, K_0 and I_0 are modified Bessel functions, and F and D are constants to satisfy the boundary conditions at the sample surface $r=R$ and at the outer radius of the heater.

For the diffusivity measurements, only the ratio of $T_{\rm ac}(r,t)$ at the two thermometers is important. This ratio is given by

$$\frac{T_{\rm ac}(r_2,t)}{T_{\rm ac}(r_1,t)} = \psi(\eta_1,\eta_2) e^{i\phi(\eta_1,\eta_2)} , \tag{19}$$

where η_i is used to denote η_{r_i} and ψ and ϕ are the respective amplitude and phase of the complex number given by

$$\psi e^{i\phi} = \frac{K_0(\eta_2\sqrt{i}) - D I_0(\eta_2\sqrt{i})}{K_0(\eta_1\sqrt{i}) - D I_0(\eta_1\sqrt{i})} . \tag{20}$$

$I_0(\eta\sqrt{i})$ represents a "reflected temperature wave" and its coefficient D is determined by the boundary condition $T_{\rm ac}(R,t)=0$. Hence,

$$D = K_0(R\eta_2\sqrt{i}/r_2)/I_0(R\eta_2\sqrt{i}/r_2) .$$

Given r_1, r_2, and R, one can find ψ and ϕ as functions of η_2. Thus, the two experimentally measured quantities ψ and ϕ provide independent determinations of η_2. From values of η_2, the thermal diffusivity is determined by the equation

$$\alpha = \Omega \frac{r_2^2}{\eta_2^2} . \tag{21}$$

If all the excitations being probed respond at rates much faster than Ω, the amplitude (ψ) and phase (ϕ) measurements should correspond to the same η_2. If, however, there is a significant amount of specific heat arising from excitations for which $\tau^{-1} < \Omega$, the diffusivity α is a complex quantity. A consequence of the imaginary component of α is that the value of η_2 determined from ψ can differ from the value determined from ϕ. This matter is discussed below, where tests at zero pressure are presented.

By choice of appropriate frequency Ω and thermometer positions r_1 and r_2, the attenuation in the sample is such that the "reflected wave" can be eliminated. In other words, if D is sufficiently small, the assumed boundary condition $T_{\rm ac}(R)=0$ is a good approximation. Thus, the measurement can be made insensitive to poor thermal contact at the cylinder surface $(r=R)$, and insensitive to the heat capacity of the cell walls. Furthermore, if the distance from the thermometers to the ends of the sample is greater than the outer radius R, the same attenuation that limits the effects of the "reflected wave" also limits the effects arising from the finite length of the sample. Determination of α with negligible effects from finite sample size is therefore possible.

C. Sample preparation and pressure cell

The sample geometry is indicated in Fig. 1. The general approach to making the SC-8 samples was as follows. Cylinders of the material were sliced in half, along the longitudinal axis. On one of the halves, the axial heater, thermometers, and associated leads were deposited. The two semicylinders were glued back together and the assembly was turned down to its final diameter. Finally, a circular end piece (made of SC-8) was attached to the bottom end of the cylinder and was used to position the electrical feedthrough. This procedure is described in more detail in Ref. 55.

The heater was made from 0.0025-cm-diam Pt-W wire. The thermometers, made from Matsushita 100-Ω resistors for use at 0.1–2 K or Allen-Bradley 10-Ω resistors for use at 2–10 K, were placed at radii $r_1 \approx 0.25$ cm and $r_2 \approx 0.50$ cm. The vapor-deposited tin thermometer leads had a superconducting transition near 3.7 K; this transition served to indicate the pressure. The heater and thermometers were all four-terminal devices. With no power applied to the heater, the carbon thermometers were calibrated *in situ* against a germanium-resistance thermometer. The germanium thermometer had been previously calibrated on the EPT 76 temperature scale against superconducting fixed points, with interpolation using magnetic thermometry.

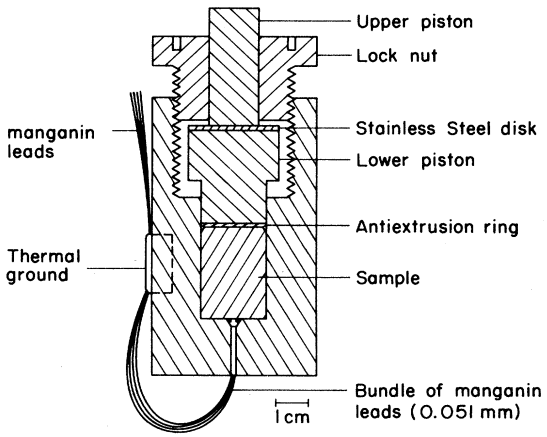

FIG. 2. Pressure cell. The notches on top of the lock nut represent threaded holes used to make mechanical and thermal contact to the cryostat.

The beryllium-copper pressure cell employed a self-clamping piston arrangement constructed as shown in Fig. 2. The cell assembly consisted of the beryllium-copper vessel and lock nut, two tungsten carbide pistons, a stainless-steel disk, a copper antiextrusion ring, and the sample and feedthrough. N grease served to fill any remaining volume of the sample chamber, in addition to providing lubrication and thermal contact to the cell. After force was applied to the pistons at room temperature, the lock nut was tightened. The upper piston could then be removed and the lock nut bolted to the cold finger of a cryostat. For measurements near 1 K and below, a ^{3}He-^{4}He dilution refrigerator was used; measurements in the range 2–10 K were performed in a pumped ^{4}He cryostat. Leads from the sample were brought up the side of the pressure cell and thermally grounded to its outer surface. Should a sample survive the pressure and temperature cycling, it could be extracted from the cell and reused.

D. Experimental conditions and estimates of errors

The chief determinants of error for the thermal conductivity measurements were the thermometer noise and the thermometer sensitivity. The small (1–3 %) temperature differences employed to measure κ required careful use of the carbon-chip thermometers. It was noticed that the carbon-chip resistance values R drifted noticeably over several hours.[56] However, the logarithmic derivative $m \equiv d(\ln R)/d(\ln T)$ was stable over the course of a run. Therefore, the values of R were checked before and after each conductivity measurement to ensure that no appreciable drift had occurred. All calculations of temperature changes made use of the stable quantity $m(R)$ and the most recently determined values of R. In this fashion, problems arising from thermometer drift were eliminated. The applied temperature gradients in the samples could be measured to roughly 1%. Errors resulting from measurement of geometrical quantities were less than 1%.

Radial heat-flow measurements of the low-temperature thermal diffusivity of SC-8 employed the ac, steady-state technique discussed above. The measurement frequency $\Omega/2\pi$ was varied as the thermal diffusivity changed with temperature. Typical measurement frequencies were 180 Hz near 0.3 K, 110 Hz near 1 K, 32 Hz near 3 K, and 0.75 Hz near 10 K. The chief sources of experimental uncertainty were the errors in determination of the relative phase and of the amplitude ratio for the two thermometer signals. These errors depended on noise in the thermometers and were estimated to be between 1% and 2% of the measured diffusivity. The error in determination of thermometer positions and sample radius would give rise to a 1% error in the thermal diffusivity.

In order to establish the reliability of the measurement techniques, tests were made at zero pressure (outside the pressure cell). We believe these tests are of major importance, as diffusive techniques can lead to erroneous results.[57] For radial heat-flow measurements of κ at zero pressure, a cylindrical sample constructed as described above was used. The sample was coated with N grease for thermal contact, and the radial cylinder surface alone was wrapped with copper foil; the end surfaces were left uncovered. Low-temperature measurements of κ were then performed. The results are shown in Fig. 3. In addition, "longitudinal" heat-flow measurements were performed on a SC-8 sample having the same batch number as that which was used to construct the cylinders. (Because of a 5–10 % uncertainty in the geometrical factor[58] for this measurement, the results were scaled by a constant factor so that they matched the earlier measurements at ~0.4 K.) As can be seen from Fig. 3, the radial and longitudinal heat-flow measurements are then in agreement with one another over the entire temperature range. These data are also in good agreement with earlier results,[44] which are included in Fig. 3.

A test was performed to ensure that the sample design provided no spurious heat leaks. Such heat leaks could arise along the vapor-deposited tin leads as they make the transition from the superconducting to the normal state near 3.7 K. Heat leaks parallel to the cylinder axis become important when thermal contact is made to the end faces of the cylinder. A longitudinal heat-flow measurement of κ was made along the axis of an actual pressure sample. The sample was turned down to a radius slightly greater than that of the outer thermometer leads. Two heaters were wound around the circumference of the cylinder. A thermometer was placed at the bottom face of the cylinder (near the electrical feedthrough), and the top face of the cylinder was thermally grounded. The points marked by solid squares in Fig. 3 are the results of these measurements. As can be seen, the measured κ agrees well with the other measurements. It can therefore be concluded that the tin leads provide no significant heat leak even above the superconducting-normal transition near 3.7 K.

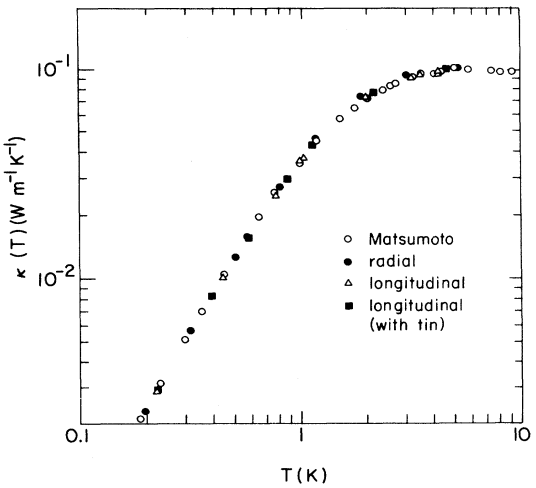

FIG. 3. Comparison of radial heat-flow measurements of thermal conductivity κ (sample 8) with longitudinal measurements, Matsumoto's data were taken from Ref. 44. The data denoted "longitudinal" are two sets of data taken with a c-clamp technique (see Ref. 58); one set is scaled by a factor 1.05, the other by a factor 0.915. Also indicated in the figure are the results (denoted "longitudinal with tin") of the test for heat leaks along the tin leads.

As a final test of the radial heat-flow measurement of κ, the effects of finite cylinder size were studied. In addition to the cylindrical surface, thermal contact was made to the top and bottom faces of the sample using N grease and copper foil, and the thermal conductivity in the plateau was measured. The apparent conductivity was $\approx 3\%$ larger when the end surfaces were covered with foil. This effect, mentioned in Sec. II A, is as expected. Hence, confidence in gained in the calculation of the effects of finite sample size and further evidence is obtained for the absence of heat leaks along the tin leads.

The thermal-diffusivity measurements were tested at zero pressure to check for agreement with more typical pulsed-calorimetry measurements. Pulsed-calorimetry measurements of C employed a standard heat-pulse technique[59] on a separate piece of SC-8. The timescale of the heat-pulse measurements was roughly 0.2 s, whereas the timescale of the ac diffusivity measurements below 1 K ranged from 4 to 12 ms.

As shown in Fig. 4, the amplitude and phase measurements of diffusivity α differ from one another below 1 K. The difference increases as temperature drops, and arises from the distribution $P(E,\tau^{-1})$ discussed previously. Also shown in Fig. 4 are computations[55] based on the tunneling model [Eq. (13)] with $\bar{P}$ as the only adjustable parameter. These computations include the phonon contribution to the specific heat. The phonons are excited much more rapidly than the experimental frequency Ω; hence they contribute only to the real part of the specific heat. An experimental specific heat may be deduced from either the phase or the amplitude measurements of α. In Ref. 55 it is shown that the average of these two specific heats is the real part of a complex specific heat. Table I compares the specific heats measured directly in a standard calorimeter on a 0.2-s time scale (C_{slow}) with those deduced from the diffusivity measurements a ≈ 5-ms time scale (C_{fast}). A comparison is also made with the tunneling model using the distribution $P(E,\tau^{-1})$ and the experimental frequencies. The computations are in agreement with the measurements.[55] In brief, the present ac measurements of specific heat agree well with those

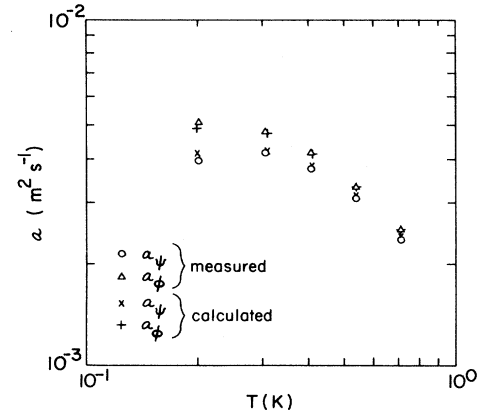

FIG. 4. Amplitude (ψ) and phase (ϕ) measurements of thermal diffusivity α below 1 K. The measurements were performed at zero pressure (sample 8). The calculations use the tunneling model distribution $P(E,\tau^{-1})$.

TABLE I. Comparison of measured and calculated values of $C_{\text{slow}}/C_{\text{fast}}$. For the measured values, column (a) used smooth curves through the data; column (b) was tabulated from fits to "slow" and "fast" data. The fit to the "slow" data gives a phonon contribution of $\approx 20T^3$ J m^{-3} K^{-1} and a value of $\approx 9 \times 10^{44}$ J^{-1} m^{-3} for $\bar{P}$. Using the same phonon contribution, the fit to the "fast" data gives the same $\bar{P}$. Alternatively, by use of both the phonon term and $\bar{P}$ from the fit to "slow" data, the 5-ms time scale is recovered when the fit is made to the "fast" data. The values in column (a) have uncertainties of roughly 2%.

T (K)	$C_{\text{slow}}/C_{\text{fast}}$ (measured) (a)	(b)	$C_{\text{slow}}/C_{\text{fast}}$ (calculated)
0.20	1.23	1.20	1.20
0.31	1.14	1.14	1.14
0.41	1.09	1.10	1.10
0.54	1.04	1.07	1.07
0.71	1.01	1.04	1.04

measured by standard calorimetric methods if the distribution in TLS relaxation times is taken into consideration.

In summary, the tests of techniques for determining κ and α at zero pressure show that these measurements respond to intrinsic behavior of the SC-8 sample. Furthermore, the effects of finite sample size are small and can be estimated for κ measurements; such effects are negligible for the diffusivity measurements. Hence, the radial heat-flow measurements of κ and α are worthy tools for investigating the low-temperature thermal properties of pressurized SC-8 samples.

E. Determination of sample pressure

As described above, a uniaxial pressure is applied to the sample cell at room temperature. As the sample is cooled, differential thermal contraction reduces the pressure on the sample. Therefore, tin transducers are embedded in the sample to measure the pressure *in situ*. However, the tin transducers can provide only relative pressure measurements. This limitation has two causes. First, the direct dependence of T_c is on volume; T_c is indirectly related to pressure through this dependence on volume. In most studies of pressure-dependent T_c's the applied pressure is hydrostatic, and hence the volume change of the superconductor is the result of compression in all three Cartesian directions. In the case of a superconductor embedded in a cylinder that is under uniaxial compression, however, the volume change is due to compression along the longitudinal axis of the cylinder. Also, if there is excess volume in the cell, initially the sample will expand to meet the inner radial and end walls of the cell. This uncertain initial deformation of the sample complicates the comparison of T_c from sample to sample, as the volume change of the tin transducers cannot easily be predicted from the applied pressure until uniaxial conditions are achieved.

The second problem with determining pressures from measured T_c's in evaporated tin is related to the thickness of the tin transducers. Although the tin leads

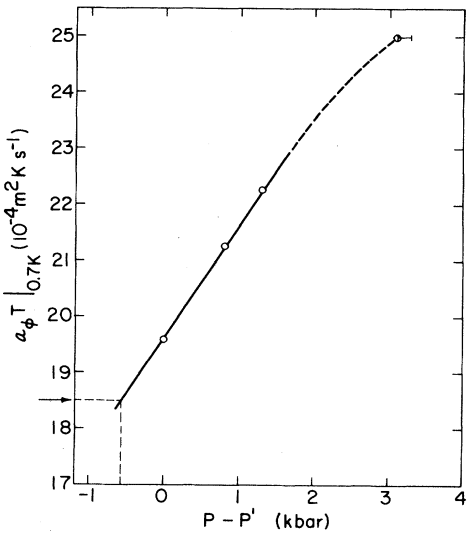

FIG. 5. The quantity $\alpha T|_{0.7\,\mathrm{K}}$ (from phase measurements) vs relative pressure $P-P'$.

employed are sufficiently thick (4000 Å) to be considered bulk, the edges of these leads may not behave as bulk tin and can affect the measured T_c's for the leads. Such behavior would depend on the conditions under which the deposition was made; hence there could be variation from sample to sample. If these effects are small, the literature value of $\partial T_c/\partial P$ for bulk tin under hydrostatic conditions should be useful in determining relative pressures in the case of uniaxial compression.

In the case of hydrostatic compression, the volume change of a sample is simply the applied pressure P divided by the bulk modulus K. In comparison, the volume change under uniaxial compression is given by the fractional change in length

$$\Delta L/L = -P/M_u \ , \tag{22}$$

where M_u is the modulus of uniaxial compression. From zero-pressure measurements at 77 K of the longitudinal and transverse sound velocities[44] for SC-8, the Poisson ratio σ is determined to be 0.33. A consequence of this value of σ is that M_u is equal to $1.5Y$, where Y is the Young's modulus. An additional consequence of $\sigma=0.33$ is that the bulk modulus and Young's modulus are equal. Therefore, for SC-8 the ratio of M_u/K is approximately 1.5. A uniaxial pressure P applied to SC-8 will induce the same volume change as a hydrostatic pressure $(K/M_u)P$. For the tin pressure sensor employed in the studies of SC-8, then, a uniaxial pressure P will cause a change in T_c indicative of an apparent hydrostatic pressure of $P/1.5$.

Assignment of relative pressures for a given sample was made by measuring ΔT_c and dividing by $\partial T_c/\partial P$ (-0.048 K/kbar for tin[60]) to find ΔP. The values of T_c were determined by monitoring the resistive transition in the tin thermometer leads and finding the midpoint of this transition. For a given run, the same T_c's were observed in both sets of thermometer leads, indicating uniformity of sample pressure.

To obtain the absolute pressure, we plot a measured parameter versus $P-P'$, where P' is the initial applied pressure, and then extrapolate to the known value of that parameter at zero applied pressure. For this purpose, it is convenient to choose a parameter which varies roughly linearly with pressure, yet is nearly independent of temperature. Such a quantity is the product αT near 0.7 K, see Fig. 5. The known value of $\alpha T = 18.5\times10^{-4}$ m^{2}K/s at 0.7 K shows that the zero of pressure on the relative pressure scale is 0.6 kbar.

The above assignment of pressures can be used to deduce the low-temperature uniaxial pressure for comparison with the uniaxial pressure applied at room temperature. The apparent pressures were simply multiplied by 1.5 to obtain the low-temperature uniaxial pressures. The applied pressure is estimated from the applied force and the sample radius. Plots of low-temperature uniaxial pressures versus applied pressures for two samples are shown in Fig. 6. The slopes of the two sets of data are nearly unity. The intercepts along the applied pressure axis indicate the effects of thermal contraction of the sample and the pressure P_0 required to fill any excess volume in the cell initially. The effects of friction would be evident as a departure from the unity slope. Indeed, near 4 kbar applied pressure, some mechanical binding was perceived during application of force to the cell. After release of pressure to roughly 2 kbar, one of the samples was eventually pressurized to 6.7 kbar, and no further binding was noticed. The important information provided by Fig. 6 is that, for the applied pressures, the cell functions as one would expect. The approximately unity slopes indicate that the assumptions made, in assigning low-temperature pressures, have been reasonable. All pressures quoted in later sections are effective hydrostatic pressures, i.e., the hydrostatic pressure required to cause the volume change as observed in the tin transducers during a given run.

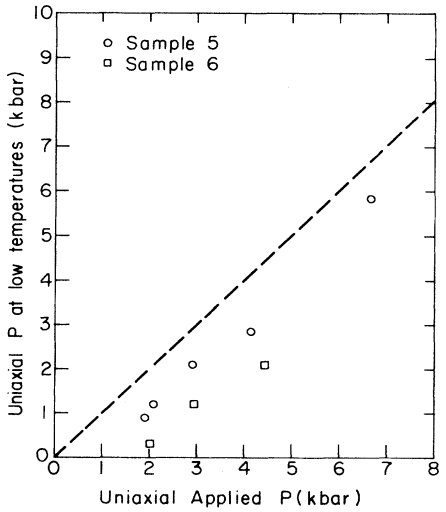

FIG. 6. Uniaxial pressure at low temperatures vs the applied (room temperature) uniaxial pressure. The differences between horizontal intercepts for samples 5 and 6 are related to differences in P_0. Thermal contraction also contributes to the horizontal intercepts.

III. EXPERIMENTAL RESULTS AND ANALYSIS

The results of the measurements of conductivity $\kappa(T)$ at several pressures are shown in Fig. 7. The most notable effect of pressure on κ appears to be that the plateau conductivity increases as pressure is applied. The pressure-dependent behavior of κ at fixed temperatures is shown in Fig. 8. The three temperatures chosen for the plots roughly correspond to the TLS regime (0.3 K), an intermediate regime (1 K), and the plateau regime (5 K). It is observed that the plateau conductivity rises as pressure increases, whereas the thermal conductivity in the TLS regime appears to decrease by a comparatively smaller amount.

The measurements of thermal diffusivity, using the ac steady-state radial heat-flow technique, for two samples at various pressures are shown in Fig. 9. In order to facilitate comparison for different pressures, the diffusivities have been plotted as $1/\alpha T^3$ versus T. From Fig. 9 it can be seen that the pressure effects are larger above 1 K than below 1 K. Some of the effect above 1 K is obviously a result of the increased plateau conductivity of Fig. 8, but it will soon be apparent that the specific heat also changes with pressure and contributes to the change in thermal diffusivity.

Using measured thermal diffusivities and graphical interpolation of the measured thermal conductivities, specific-heat data were computed. The calculated specific-heat data, plotted as C/T^3, are shown in Fig. 10. Application of pressure causes a decrease in specific heat. The relative magnitude of this decrease is nearly constant over the entire temperature region studied. In order to emphasize the rather uniform changes in specific heat with pressure, the specific-heat data, scaled by constant factors, are replotted in Fig. 11. The pressure dependence at fixed temperatures is displayed in Fig. 12. As discussed in Sec. I, data below 1 K [Fig. 12(a)] reflect primarily the behavior of TLS's and phonons; the data at 4 and 6 K in Fig. 12(b) relate primarily to phonons and the excitations responsible for the bump in C/T^3. The effect of pressure is essentially the same at all temperatures, except on the low-temperature side of the bump near 4 K.

The analysis of the data is organized as follows. First, the data for temperatures below 1 K are analyzed in the context of the tunneling model. The results of this analysis are then compared to earlier results for SiO_2. Next, the data for temperatures above 1 K in the "bump" and "plateau" regimes are analyzed, and qualitative comparisons are made with the structural models of KBr-KCN and SiO_2 as well as the fracton theory. The measurements in the bump and plateau regimes are also compared to the earlier results for Teflon.

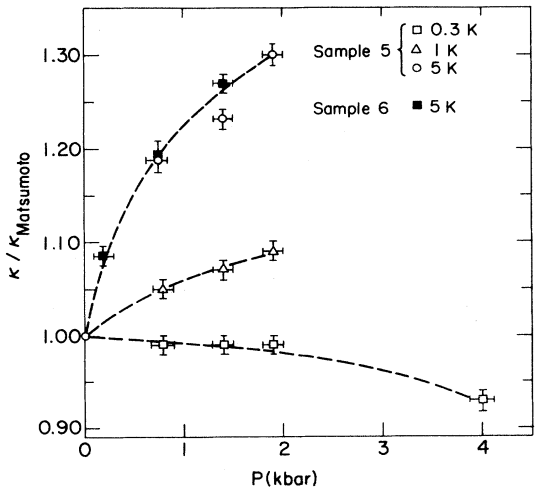

FIG. 8. Thermal conductivities, normalized to zero-pressure values, plotted as a function of pressure for three temperatures.

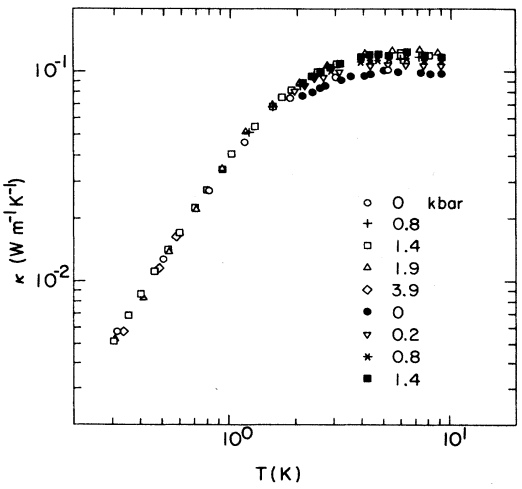

FIG. 7. Low-temperature thermal conductivity of SC-8 at several pressures. The zero-pressure data are from sample 8 (open circles) and Matsumoto (solid circles). Data sets extending below 1 K are from sample 5; those curves having points only in the plateau regime are from sample 6.

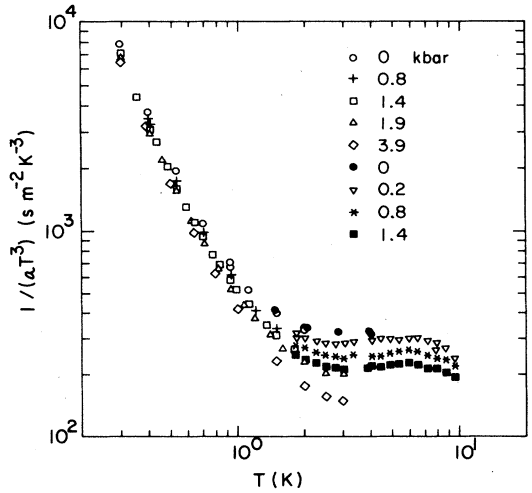

FIG. 9. Low-temperature thermal diffusivity of SC-8 at several pressures, plotted as $1/\alpha T^2$ vs T. The data are from sample 5 (0.3–3 K) and sample 6 (2–10 K). The zero-pressure data above 3 K (solid circles) are calculated from heat-pulse measurements of C and Matsumoto's measurements of κ. Data from samples 5 and 6 are phase measurements of the thermal diffusivity.

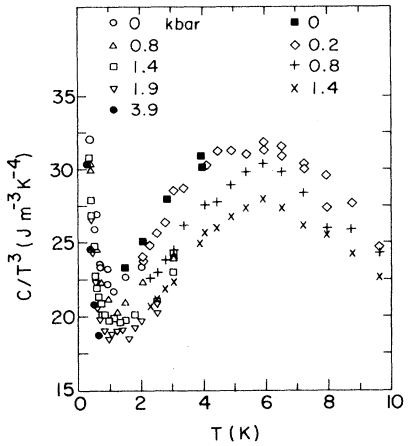

FIG. 10. Pressure-dependent specific heat of SC-8 at low temperature. The specific heat is calculated from the measured thermal conductivity (Fig. 7) and the measured thermal diffusivity (Fig. 9). The points indicated by solid squares are from heat-pulse calorimetric measurements.

A. The TLS regime ($T < 1$ K)

For temperatures below 1 K the dominant excitations are believed to be phonons and TLS's. Hence, fits using a term quasilinear in temperature and a T^3 term can be made for the data[61] taken at temperatures below 1 K. When such fits (described below) were applied to previous[46] data for the specific heat of SC-8, the resulting T^3 term was only 7% greater than the phonon contribution calculated from the low-temperature sound velocities. Hence, the T^3 term (denoted B below) can be considered to arise *predominantly* from phonons.

The form to which specific-heat data were fitted below 1 K is given by

$$\frac{C}{T^3}=\frac{\pi^2}{12}k_B^2\bar{P}T^{-2}\ln\left[\frac{4t}{\tau_{\min}}\right]+B\ , \tag{23}$$

where t is the time scale of the measurement, $\tau_{\min}$ is given by Eq. (6) evaluated at $E=2k_BT$, $\bar{P}$ is the TLS energy density, and B is the Debye phonon specific heat divided by T^3. The logarithmic term in Eq. (23) gives rise to a superlinear (e.g., $T^{1+\alpha}$) dependence of C on T. The details of the fitting procedure can be found in Ref. 55, where a check of the procedure is presented. Once tested for proper behavior at zero pressure, the fit of Eq. (23) to zero-pressure data was used for comparison with data measured under applied pressure. Specifically, the specific-heat data for a given pressure and given temperatures below 1 K were divided by zero-pressure specific-heat values generated from the aforementioned fit. The results of this comparison are tabulated in Table II, from which it can be seen that pressure-induced changes in C amount to a constant factor for $T<1$ K. These constant factors are expressed as values (relative to $P=0$) of $\bar{P}$ and B in Table III.

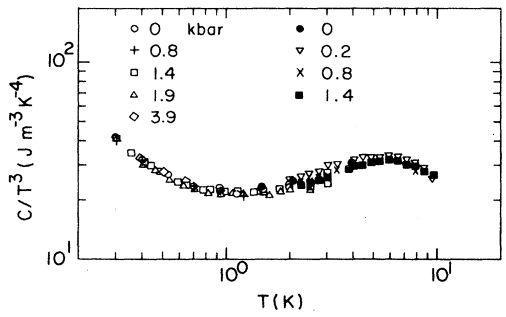

FIG. 11. Specific-heat data at various pressures scaled by constant factors (Table III, column 5) to show the uniform changes with pressure.

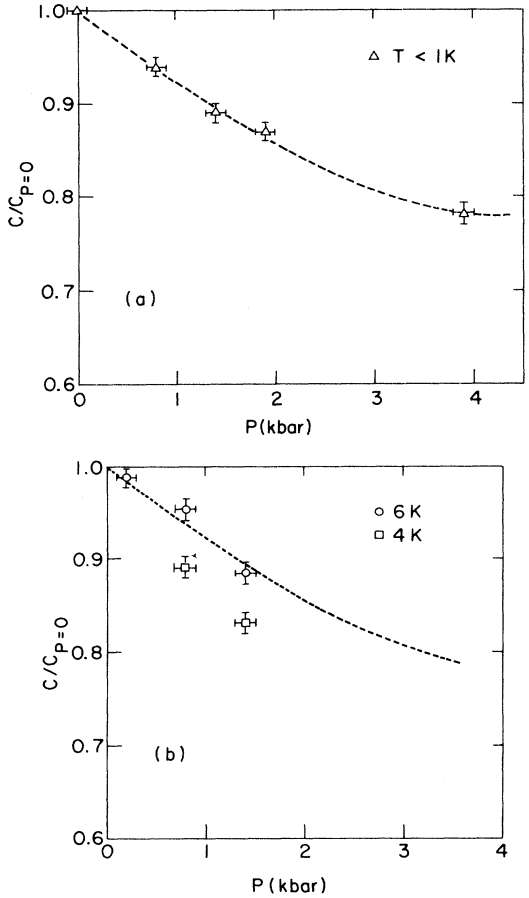

FIG. 12. Normalized specific heat as a function of pressure (a) for temperatures below 1 K and (b) for temperatures (4 and 6 K) near the maximum in C/T^3. Because no $P=0$ data are available at 6 K, the 6-K data are normalized at $P=0.2$ kbar. From data for $T<6$ K an estimate of $C_{0.2\text{ kbar}}/C_0\approx 0.98$ is made. The data $C_p/C_{0.2\text{ kbar}}$ are then multiplied by this factor of 0.98. The dashed line in (b) represents the data in (a) for convenience of comparison.

In Sec. I A it was shown that the assumptions of the tunneling model give the result that the TLS contribution

TABLE II. Specific heat C of SC-8 below 1 K, normalized to zero-pressure values, C_0. Data are from sample 5.

0.8 kbar		1.4 kbar		1.9 kbar		3.9 kbar	
T (K)	C/C_0	T (K)	C/C_0	T (K)	C/C_0	T (K)	C/C_0
0.306	0.942	0.305	0.909	0.355	0.883	0.305	0.778
0.405	0.936	0.360	0.884	0.412	0.854	0.394	0.779
0.413	0.961	0.415	0.895	0.467	0.856	0.506	0.784
0.539	0.925	0.441	0.904	0.540	0.850	0.646	0.793
0.713	0.950	0.494	0.894	0.631	0.854		
		0.541	0.866	0.716	0.899		
		0.597	0.880	0.828	0.863		
		0.650	0.888				
		0.708	0.900				
		0.782	0.897				
		0.844	0.919				
Avg:	0.943±0.014	Avg:	0.894±0.014	Avg:	0.865±0.018	Avg:	0.783±0.014

to the low-temperature specific heat and thermal resistivity can be expressed in terms of the parameters $\bar{P}$ and γ. If an amorphous solid retains its glassy nature as pressure is applied, the pressure-induced changes in thermal properties should reflect the pressure dependences of these two parameters. It shall be seen that within this framework the tunneling model can account for the observed behavior. Furthermore, this strict application of the tunneling model will reveal some interesting correlations.

The fact that, below 1 K, the specific heat changes simply by a constant factor from pressure to pressure makes determination of the relative (i.e., normalized to the zero-pressure value) TLS density quite easy. Table III provides relative magnitudes of $\bar{P}$ *assuming* that $\ln(4t/\tau_{\min})$ does not change significantly with pressure.

Another consequence of the constant-factor changes in specific heat with pressure is that values of phonon velocity v, normalized to the zero-pressure value, can be found. If the T^3 term is predominantly a phonon specific heat, as is the case for SC-8, then $B \propto 1/v^3$. Hence, the percent changes in $1/v^3$ with pressure are the same as for $\bar{P}$. Also, values of ρ, normalized to the zero-pressure value, were calculated from estimates of the changes in sample volume upon compression. These volume estimates were made[55] from measurements[62] of the pressure dependence of the longitudinal sound velocity in SC-8. The computed values of v and ρ are included in Table III.

For the purposes of using the tunneling model to analyze the thermal-conductivity data, results for the lowest temperatures (near 0.3 K) were chosen. The nearly-pressure-independent values of thermal conductivity κ (0.3 K) were used with the pressure-dependent v and ρ to determine the normalized values of the coupling parameter $\bar{P}\gamma^2$. In addition, the above-mentioned values of $\bar{P}$ were used to find normalized values of γ^2. The results, tabulated in Table III, show that the TLS-phonon coupling, as represented by either $\bar{P}\gamma^2$ or γ^2, increases as pressure is applied. Also shown in Table III are the normalized values of $\gamma^2/\rho v^5$ for the various pressures. As this quantity does not change significantly with pressure, the logarithmic term $\ln(4t/\tau_{\min})$ in the TLS specific heat can be considered pressure independent. Therefore the values of $\bar{P}$, as determined from specific-heat data, need no correction for changes in $\tau_{\min}$.

To summarize the above results, strict application of the tunneling model to the SC-8 data indicates that the energy density $\bar{P}$ of TLS's decreases with pressure, whereas the coupling (γ or $\bar{P}\gamma^2$) between phonons and TLS's increases with pressure. Furthermore, it is found that the form of $\tau_{\min}$ is unchanged by pressure. These trends are obtained assuming that the distribution $P(E,\tau^{-1})$, as given by the tunneling model, applies to SC-8 at all pressures studied.[63]

The decrease in $\bar{P}$ can be interpreted in two ways. Either the number of TLS's could be changing with pressure, or the same number of TLS's may be spread out over a broader range of energies. The second interpretation will be mentioned later, when the response to pressure of the "bump" in C/T^3 is discussed.

From Table III one may observe that the enhanced

TABLE III. Values of various tunneling model parameters for measurements under pressure on sample 5. All data (except pressures) are normalized to zero-pressure values. The uncertainties quoted for $\bar{P}$ or B are one standard deviation. The normalized $\bar{P}$ or B are from specific-heat data; the normalized $\rho v/\bar{P}\gamma^2$ are from thermal-conductivity data taken at 0.3 K. Normalized values for ρ are calculated from estimates of sample compression and those for v are calculated from B ($\propto 1/v^3$).

P (kbar)	ρ	v	ρv^2	$\bar{P}$ or B	$\rho v/\bar{P}\gamma^2$	$\bar{P}\gamma^2$	γ^2	$\gamma^2/\rho v^5$
0	1.00	1.00	1.00	1.00	1.00	1.00	1.00	1.00
0.8	1.030	1.021	1.074	0.94±0.01	0.99±0.01	1.06	1.13	0.99
1.4	1.041	1.040	1.111	0.89±0.01	0.99±0.01	1.09	1.22	0.98
1.9	1.047	1.048	1.150	0.87±0.02	0.99±0.01	1.11	1.27	0.96
3.9	1.081	1.086	1.274	0.78±0.01	0.93±0.01	1.26	1.62	0.99

coupling between phonons and TLS's as pressure is applied suggests the proportionality $\bar{P}\gamma^2 \propto \rho v^2$; that is, a relationship between $\bar{P}\gamma^2$ and an elastic constant. Such a correlation was proposed theoretically by Klein *et al.*[64] It is interesting to note that the pressure dependence of specific heat, which gives $B \propto \bar{P}$, suggests another correlation, namely $\bar{P} \propto v^{-3}$. When this proportionality is used with $\bar{P}\gamma^2 \propto \rho v^2$, the relation $\gamma^2 \propto \rho v^5$ is obtained. This proportionality was implied earlier, when it was mentioned that $\tau_{\min}$ is roughly constant with pressure. The correlation $\bar{P} \propto v^{-3}$ can also be expressed as $\bar{P} \propto \rho/\Theta_D^3$, where Θ_D is an effective Debye temperature.

A comparison of the measurements on SC-8 with those on vitreous silica can now be made. The pressure-dependent ultrasonic attentuation[37] in SiO_2 reveals increased attenuation as pressure is applied, which is in qualitative agreement with the increased TLS-phonon coupling observed in SC-8 under pressure. The authors of the SiO_2 work, however, attribute[37] the increased coupling to an increased TLS density $\bar{P}$. The measurements on SC-8, on the other hand, suggest a decrease in $\bar{P}$ with pressure. In short, the experiments on SiO_2 appear to be in qualitative agreement with those on SC-8 although the respective interpretations are not in agreement. It should be mentioned that there were some technical difficulties (related to bonding between transducers and sample[65]) for the SiO_2 measurements. Hence, a comparison between SC-8 studies and the SiO_2 measurements may not be valid.

B. The "bump" and "plateau" ($1 \lesssim T \lesssim 10$ K)

It was noted that the pressure-induced changes in C/T^3 near 4 K are more pronounced than at 6 K. Such behavior is consistent with a shift of bump excitations to higher energies. The density of states responsible for the bump has a rather sharp rise with frequency. Therefore, the effects of an upward energy shift of this group of excitations should indeed be more pronounced for the low-temperature side of the bump. In contrast, an increase in a cutoff energy, such as a maximum TLS energy or the Debye temperature Θ_D, causes a *uniform* drop in C/T^3 in the relevant temperature range. Also, the link, implied by microscopic models, between TLS's and the excitations responsible for the bump, suggests that an increase in energy scale of the bump should bring about an increase in the upper limit of TLS energies. Such ideas could account for the observed decrease in TLS density as pressure is applied. In addition, an apparent correlation between the TLS density and the Debye temperature was noted in the preceding section. Hence, the concurrent decreases in TLS, phonon, and bump specific heats suggest that the three types of excitations may all be manifestations of the same basic vibrational structure.

Applied pressure brings about an increase in the plateau thermal conductivity and a decrease in the bump in C/T^3. The microscopic models of librational modes in KBr-KCN and rotational modes in SiO_2 can predict these qualitative results. In addition, the reduction of sample volume should cause the same effects according to the fracton theory. From all of these models, one would expect an increase in energy scale of the bump and plateau as the sample elastic constants stiffen.

It was mentioned in Sec. I B that phonon scattering in the plateau regime may be characterized by $l^{-1} = A\omega^4$, where l is a phonon mean free path and ω is a phonon frequency. Freeman and Anderson[66] found an empirical correlation between the scattering strength A and phonon velocity v in glasses, namely $A \propto v^{-4}$ or $l \propto \lambda^4$. This behavior suggests the presence of Rayleigh scattering of phonons by some structure in the glass. If this relation for A is substituted into the expression for thermal conductivity, one finds that the thermal conductivity in the plateau should obey the relation $\kappa_{\text{plateau}} \propto v^2$. It should be mentioned that the magnitude of the plateau conductivity is also affected by low-frequency phonons from the TLS regime.[67] If the scattering from TLS's changes with pressure, some change in the plateau magnitude would result. Since the measured κ decreases only rather weakly with pressure at 0.3 K (Fig. 8), the increase in plateau thermal conductivities as pressure is applied may be used to obtain a reasonable estimate of the change in Av^4 with pressure.

The observed change in $\kappa_{\text{plateau}}/v^2$ versus volume is found[55] to be $\kappa_{\text{plateau}}/v^2 \propto (\text{volume})^{-\beta}$, where β is roughly 3 or 4. In terms of a possible structural length ξ, then, we find $\kappa_{\text{plateau}}/v^2 \propto \xi^{-3\beta}$, which gives $A \propto \xi^{3\beta}/v^4$. By contrast, Rayleigh scattering from structure[33] of size ξ should give $A \propto \xi^3/v^4$. Thus, it would appear that the observed scattering strength A has much too strong a dependence on ξ, implying that phonon scattering is not directly related to any structural length scales in the glass. This conclusion has been obtained in previous publications[7] where calculated magnitudes of scattering were insufficient to explain the plateau in κ.

Whereas the microscopic theories suggest that phonon localization is a consequence of interaction between bump excitations and phonons, the fracton concept suggests that phonon localization at the phonon-fracton crossover brings about the bump and plateau. If the fracton concept (or some other localization theory) is valid, the changes in plateau conductivity and sound velocity with pressure should be related to changes in a structural length scale ξ. The fracton theory makes a prediction as to the scaling between sound velocity and length scale ξ, see Eq. (15). From the values given in Table III for v at several pressures, it is found that $v \sim \xi^{-3}$, i.e., $\theta = 6$. For percolation problems, Alexander and Orbach[34] obtained values of 2 for θ, while experiments on dilute amorphous magnets[68] have given values of 1.5 for θ. Brillouin-scattering measurements on silica aerogels[69] give $\theta \approx 1.8$. Therefore, the value of 6 for θ seems significantly higher than has been calculated or measured for fractal systems, although the qualitative nature of the fracton theory prevents a theoretical estimate of an upper bound on θ. As has been the case for many attempts to test the fracton theory, the experimental results presented here are inconclusive. There is certainly qualitative agreement between theory and experiment; however, no real quantitative test is possible.

In summary, the apparently strong volume dependences of v and $\kappa_{\text{plateau}}/v^2$ suggest that the bump and pla-

teau features cannot be related to structural length scales. Hence, the fracton model[70] and other theories relating phonon localization to structural length scales may not be appropriate for bulk glasses. One concludes that the experiments on SC-8 favor the microscopic models.

Finally, we make a brief comparison with the measurements on Teflon mentioned earlier. The basic qualitative features of the pressure dependence of the bump in C/T^3 are the same for both SC-8 and Teflon. In particular, both materials exhibit a reduction of the bump as pressure is applied. Furthermore, both materials stiffen with pressure, as expected, and as indicated by the decrease in the T^3 contribution to the specific heat. Quantitative comparisons, carried out in Ref. 55, reveal only subtle differences that may arise from the pressure-dependent partial crystallinity of Teflon.

IV. CONCLUSIONS

The thermal properties of the amorphous polymer SC-8 were measured as a function of pressure in the temperature range 0.3–10 K. Data for temperatures below 2 K were collected for pressures to 3.9 kbar; data in the range 2–10 K were collected for pressures to 1.4 kbar. These measurements probed the quasilinear temperature dependence of the specific heat and the roughly T^2 thermal conductivity at temperatures below 1 K, and the "bump" and "plateau" regimes at higher temperatures. The purpose of the study was to examine the strain dependence of the various excitations responsible for these features, and to look for possible length-scale dependences. An additional motivation for the work was to examine possible correlations between the various features in the low-temperature thermal properties of a glassy solid.

During the course of zero-pressure measurements, a reconfirmation of the time-dependent glassy specific heat was made. Calculations using the tunneling-model distribution $P(E,\tau^{-1})$ could account for the observed differences between the short-time ($\sim$5 ms) amplitude and phase measurements of thermal diffusivity below 1 K. In addition, differences between the short-time measurements and "heat-pulse" (0.2 s) measurements were explained by the same calculations.

Relative to unstrained SC-8, samples under pressure were observed to have larger thermal conductivity κ in the plateau regime, a smaller κ near 0.3 K, and a smaller specific heat at all temperatures. The specific heat changed rather uniformly over the entire temperature range studied, except for temperatures near 4 K, where the changes were more pronounced.

In terms of the tunneling model,[71] the data obtained below 1 K could be accounted for by a decrease in the TLS density $\bar{P}$ and an increase in the phonon coupling constant γ as pressure increases. In this analysis, the product $\bar{P}\gamma^2$ exhibited a proportionality with elastic constants; that is, $\bar{P}\gamma^2 \propto \rho v^2$. Furthermore, the uniform decrease in specific heat with pressure revealed the correlation $\bar{P} \propto \rho/\Theta_D^3$, where Θ_D is an effective Debye temperature.

Microscopic models of KBr-KCN and SiO_2 suggest the above-mentioned qualitative behavior of the bump and plateau with pressure. Furthermore, the models suggest that the TLS's are low-energy modes of the same basic vibrational structure as those responsible for the bump. In light of such suggestions, the decrease in $\bar{P}$ with pressure can be understood as an increase in some maximum energy for TLS's such that the total number of TLS's remains fixed.

As the pressure dependence of specific heat was found to be similar for TLS's and phonons, the measurements suggest that these excitations may be related.[72] The apparent shift of bump excitations to higher energies and the concurrent decrease in $\bar{P}$ support the notion that the bump excitations and TLS's are related. In addition, the concurrent increase in plateau thermal conductivity and decrease in bump specific heat support the idea that the bump and plateau phenomena are related. In brief, one can speculate that all the low-energy excitations in this amorphous polymer appear to be interrelated.

Theories of phonon localization, fractal or otherwise, also make qualitative predictions which appear to be in agreement with the experimental observations. However, the quantitative results do not support these theories. The dependence of the plateau thermal conductivity and phonon velocity on sample volume appear to be stronger than can be predicted by theories based on structural length scales.

ACKNOWLEDGMENTS

Support was provided in part by the U.S. National Science Foundation (Low Temperature Physics Program) under Grant No. DMR-86-13630. Measurements of the pressure-dependent ultrasonic velocity in SC-8 were kindly provided by Professor Nikolas I. Christensen of the Department of Earth and Atmospheric Science at Purdue University. One of us (J.M.G.) is grateful for the financial support that Eastman Kodak has provided.

*Present address: IBM Research Division, Thomas J. Watson Research Center, P.O. Box 218, Yorktown Heights, NY 10598.

[1]R. C. Zeller and R. O. Pohl, Phys. Rev. B **4**, 2029 (1971).
[2]J. J. Freeman and A. C. Anderson, Phys. Rev. B **34**, 5684 (1986).
[3]For a general review, see *Amorphous Solids*, edited by W. A. Phillips (Springer, Berlin, 1981).
[4]B. Golding, J. E. Graebner, B. I. Halperin, and R. J. Schutz, Phys. Rev. Lett. **30**, 223 (1973).
[5]P. W. Anderson, B. I. Halperin, C. M. Varma, Philos. Mag. **25**, 1 (1971).
[6]W. A. Phillips, J. Low Temp. Phys. **7**, 351 (1971).
[7]D. P. Jones, N. Thomas, and W. A. Phillips, Philos. Mag. B. **38**, 271 (1978).
[8]H. v. Löhneysen, Phys. Rep. **79**, 161 (1981).
[9]U. Buchenau, N. Nücker, and A. J. Dianoux, Phys. Rev. Lett. **53**, 2316 (1984).

[10]M. P. Zaitlin and A. C. Anderson, Phys. Status Solidi B **71**, 323 (1975).
[11]P. F. Tua, S. J. Putterman, and R. Orbach, Phys. Lett. **98A**, 357 (1983).
[12]E. R. Grannan, M. Randeria, and J. P. Sethna, Phys. Rev. Lett. **60**, 1402 (1988).
[13]U. Buchenau, M. Prager, N. Nücker, A. J. Dianoux, N. Ahmad, and W. A. Phillips, Phys. Rev. B **34**, 5665 (1986).
[14]J. Jäckle, Z. Phys. **257**, 212 (1972).
[15]J. L. Black, Phys. Rev. B **17**, 2740 (1978).
[16]H. v. Löhneysen, H. Rüsing, and W. Sander, Z. Phys. B **60**, 323 (1985).
[17]M. Rothenfusser, W. Dietsche, and H. Kinder, Phys. Rev. B **27**, 5196 (1983).
[18]D. P. Jones and W. A. Phillips, Phys. Rev. B **27**, 3891 (1983).
[19]D. Moy, J. N. Dobbs, and A. C. Anderson, Phys. Rev. B **29**, 2160 (1984).
[20]J. J. De Yoreo, W. Knaak, M. Meissner, and R. O. Pohl, Phys. Rev. B **34**, 8828 (1986), and references cited therein.
[21]P. Vinet, J. R. Smith, J. Ferrante, and J. H. Rose, Phys. Rev. B **35**, 1945 (1987).
[22]M. Randeria (private communication). The objection might be raised that the above theory, relevant to $KBr_{1-x}(CN)_x$, may not be applicable to amorphous materials in general. It should therefore be mentioned that the authors of this model have generalized it in terms of two parameters—the density of elastic dipole defects and the associated dipole moment. With these two parameters and data on vitreous silica, fits were made to the measured density of states (from neutron-scattering data) and measured thermal conductivity. The authors have claimed that from the dipole density and dipole moment, as determined from the fit to the neutron-scattering measurements, the dipole-defect theory roughly predicts the correct thermal conductivity.
[23]L. Guttman and S. M. Rahman, Phys. Rev. B **33**, 1506 (1986).
[24]U. Buchenau, Solid State Commun. **56**, 889 (1985).
[25]A. Aharony, S. Alexander, O. Etin-Wohlman, and R. Orbach, Phys. Rev. B **31**, 2565 (1985).
[26]Y. Gefen, A. Aharony, and S. Alexander, Phys. Rev. Lett. **50**, 77 (1983).
[27]R. Vacher, T. Woignier, J. Pelous, and E. Courtens, Phys. Rev. B **37**, 6500 (1988).
[28]Y. Tsujimi, E. Courtens, J. Pelous, and R. Vacher, Phys. Rev. Lett. **60**, 2757 (1988).
[29]D. W. Schaefer and K. D. Keefer, Phys. Rev. Lett. **56**, 2199 (1986).
[30]S. K. Mitra and R. W. Hockney, J. Phys. C **13**, L739 (1980).
[31]R. Orbach and H. M. Rosenberg, in *Proceedings of the 17th International Conference on Low-Temperature Physics–LT-17,* edited by U. Eckern, A. Schmid, and H. Wuhl (Elsevier, Amsterdam, 1984), p. 375; Raman-scattering measurements are reported by A. Boukenter, E. Duval, and H. M. Rosenberg, J. Phys. C **21**, 541 (1988). See also P. P. Lottici, Phys. Status Solidi B **146**, K81 (1988).
[32]D. E. Farrel, J. E. de Olivera, and H. M. Rosenberg, in *Phonon Scattering in Condensed Matter,* edited by W. Eisenmenger (Springer-Verlag, Berlin, 1983), p. 422. See also M. Arai and J. E. Jorgensen, Phys. Lett. **133**, 70 (1988).
[33]J. E. Graebner, B. Golding, and L. C. Allen, Phys. Rev. B **34**, 5696 (1986).
[34]S. Alexander and R. Orbach, J. Phys. (Paris) Lett. **43**, L625 (1982).
[35]T. L. Smith, J. R. Matey, and A. C. Anderson, Phys. Chem. Glasses **17**, 214 (1976).
[36]J. D. Boyer, J. C. Lasjaunias, R. A. Fisher, and N. E. Phillips, J. Non-Cryst. Solids **55**, 413 (1983).
[37]U. Bartell and S. Hunklinger, J. Phys. (Paris) Colloq **43**, C9-489 (1982).
[38]J. D. Boyer, Ph.D. thesis, University of California, Berkeley, 1982.
[39]J. N. Dobbs and A. C. Anderson, J. Non-Cryst. Solids **69**, 429 (1985).
[40]S. Hunklinger, Cryogenics **28**, 224 (1988).
[41]A. C. Anderson, J. Non-Cryst. Solids **85**, 211 (1986).
[42]J. J. Freeman, J. X. Mack, and A. C. Anderson, J. Non-Cryst. Solids **86**, 407 (1986).
[43]*Treatise on Adhesion and Adhesives,* edited by R. L. Patrick (Dekker, New York, 1969), Vol. 2, p. 78.
[44]D. S. Matsumoto, Ph.D. thesis, University of Illinois at Urbana-Champaign, 1980.
[45]S. Kelham and H. M. Rosenberg, J. Phys. C **14**, 1737 (1981).
[46]D. S. Matsumoto, C. L. Reynolds, Jr., and A. C. Anderson, Phys. Rev. B **19**, 4277 (1979).
[47]O. Sandberg, P. Andersson, and G. Bäckström, J. Phys. E **10**, 474 (1977).
[48]P. Andersson and G. Bäckström, Rev. Sci. Instrum. **47**, 205 (1976).
[49]J. H. Blackwell, J. Appl. Phys. **25**, 137 (1954).
[50]E. P. Roth and A. C. Anderson, J. Appl. Phys. **47**, 3644 (1976).
[51]P. Andersson and G. Bäckström, High Temp.-High Pressures **4**, 101 (1972).
[52]D. S. Matsumoto, C. L. Reynolds, Jr., and A. C. Anderson, Phys. Rev. B **16**, 3303 (1977).
[53]P. Andersson and G. Bäckström, J. Appl. Phys. **44**, 705 (1973).
[54]R. Berman, *Thermal Conduction in Solids* (Oxford University Press, Oxford, 1979), p. 4.
[55]J. M. Grace, Ph.D. thesis, University of Illinois at Urbana-Champaign, 1988.
[56]W. L. Johnson and A. C. Anderson, Rev. Sci. Instrum. **42**, 1296 (1971).
[57]See, for example, E. J. Cotts and A. C. Anderson, Phys. Rev. B **24**, 7329 (1981).
[58]Two attempts were made to measure the thermal conductivity of longitudinally strained rods of SC-8 epoxy by placing them in copper C clamps. With the four thermometers employed, it was determined that the thermal contact between clamps and cylinders was poor, indicating that the samples had relaxed. Because of the poor contact, the end surfaces of the cylinders could not be expected to be in complete contact with the clamps. Hence, the measured geometrical factors for the rods were believed to be in error. Indeed, it was observed that the thermal-conductivity data from these experiments differed by constant factors from run to run. The two sets of data were scaled so as to agree with Matsumoto's measurements at 0.4 K. The multiplicative factors were 0.915 and 1.05 for the two runs.
[59]G. Sellers and A. C. Anderson, Rev. Sci. Instrum. **45**, 1256 (1974).
[60]This value is an average of values found in the following references: L. D. Jennings and C. A. Swenson, Phys. Rev. **112**, 31 (1958); T. F. Smith, C. W. Chu, and M. B. Maple, Cryogenics **9**, 53 (1969); and C. A. Swenson, in *Metallurgy at High Pressures and High Temperatures,* edited by K. A. Gschneidner, Jr., M. T. Hepworth, and N. A. D. Parlee (Gordon and Breach, New York, 1964), pp. 190–195.
[61]Fits of this type seem to work fairly well for amorphous polymers, possibly because these materials have smaller "bump"

specific heats, relative to the total specific heats, than are found in inorganic glasses such as SiO_2. In Ref. 11 it is also claimed that there is fair agreement between fits and sound-velocity data for amorphous polymers.

[62]Measurements of the longitudinal sound velocity of SC-8 as a function of hydrostatic pressure were provided by Professor Nikolas I. Christensen.

[63]If this assumption is relaxed, the experimental results still support the interpretation that the form $P(E,\tau^{-1})$ changes little with pressure, as the quaslinear specific heat and nearly quadratic thermal conductivity persist under applied pressure. This argument is presented in Ref. 55.

[64]M. W. Klein, B. Fischer, A. C. Anderson, and P. J. Anthony, Phys. Rev. B **18**, 5887 (1978).

[65]S. Hunklinger (private communication).

[66]J. J. Freeman and A. C. Anderson, in *Phonon Scattering in Condensed Matter V,* edited by A. C. Anderson and J. P. Wolfe (Springer-Verlag, Berlin, 1986), p. 32.

[67]M. P. Zaitlin and A. C. Anderson, Phys. Rev. B **12**, 4475 (1975).

[68]M. B. Salamon and Y. Yeshurun, Phys. Rev. B **36**, 5643 (1987).

[69]E. Courtens, J. Pelous, J. Phalippou, R. Vache, and T. Woignier, Phys. Rev. Lett. **58**, 128 (1987).

[70]The same conclusion has been obtained from neutron-scattering measurements on amorphous Ge: U. Buchenau, M. Prager, W. A. Kamitakahara, H. R. Shanks, and N. Nucker, Europhys. Lett. **6**, 695 (1988).

[71]An extension of the tunneling model predicts a decrease in TLS specific heat with increasing pressure for network glasses, due to a reduction in effective coordination number. See M. I. Klinger, Phys. Rep. **165**, 275 (1988), and papers cited therein.

[72]A similar correlation between phonon specific heat and TLS specific heat was noticed in comparison of the specific heat of a sol-gel glass to that of vitreous silica [see J. M. Grace and A. C. Anderson, Phys. Rev. B **33**, 7186 (1986)]. The sol-gel material had phonon velocities that were a factor of 2 slower than for bulk vitreous silica. Near 1 K, the specific heat was an order of magnitude higher for the sol-gel than for the bulk glass. At lower temperatures, the sol-gel specific heat was as much as 15 times that of the bulk glass. (The apparent increase in the ratio at lower temperatures may arise from TLS's associated with residual solvent trapped in the sol-gel material.) The point to be emphasized is that the acoustically softer material exhibited a higher specific heat for temperatures near and below 1 K.